International Conference on Computational Methods in Marine Engineering
MARINE 2011
L.Eça, E. Oñate, J. García, T. Kvamsdal and P. Bergan (Eds)

NUMERICAL SIMULATION ON HYDROELASTIC RESPONSE OF STRUCTURE UNDER IMPACT LOAD FROM WATER USING EULERIAN SCHEME WITH LAGRANGIAN PARTICLES

H. MUTSUDA*, S. BASO*, K. KAWAKAMI*, K.HASHIHIRA* AND Y.DOI*

* Division of Energy and Environmental Engineering,
Faculty of Engineering, Hiroshima University
1-4-1 Kagamiyama Higashi-Hiroshima, Hiroshima, 739-8527
e-mail: mutsuda@naoe.hiroshima-u.ac.jp, web page: http://home.hiroshima-u.ac.jp/mutsuda/

Key words: Hydroelasticity, Slamming, Impact pressure, Eulerian- Lagrangian scheme

Summary. Hydroelasticity caused by water impact is of concern in many applications of ocean engineering/naval architect and a complicated physical phenomenon. We have developed a coupled Eulerian scheme with Lagrangian particles to combine advantages and to compensate disadvantages in both grid based method and particle based method. In this study, the developed numerical model was applied to hydroelastic problems due to impact pressure such as water entry of an elastic cylinder and elastic tanker motion in wave. We showed the numerical results which is overall agreement with experimental results.

1 INTRODUCTION

Hydroelasticity caused by water impact is of concern in many applications of ocean engineering/naval architect and a complicated physical phenomenon. The impact load due to a slamming can result in substantial damage in an ocean structure and a ship. Therefore, several works have been performed to predict the impact pressure acting on an ocean structure and a ship.

An extremely large load between water and a structure can cause effects of important local dynamic hydroelastic. Haugen [1] suggested that air-cushion effects may be important when there are several dominant natural periods of structural vibrations. Kvalsvold et al.[2] have already studied wave impact on elastic beams. Faltinsen [3] studied an approximate three-dimensional theoretical investigation of hydroelastic wetdeck slamming. The hydroelastic slamming problem must be hydrodynamically studied from a structural point of view [4]. For this reason, a numerical method that takes into consideration of fluid-structure interaction coupling must be developed.

Under this background, we have developed a coupled Eulerian scheme with Lagrangian particles to combine advantages and to compensate disadvantages in both grid based method and particle based method. The model has two kinds of Lagrangian particles, i.e. SPH and free surface particle on Eulerian grids to correct interface tracking error. The developed model has already applied to several kinds of fluid-structure interaction problems [5-7]. In this study, the developed numerical model is applied to hydroelastic problems due to impact pressure such as water entry of an elastic cylinder, a floating motion of elastic

structure in wave. We investigate the validation and verification of the develped model in hydroelastic problems.

2 CONPUTATIONAL METHOD

2.1 Capturing techniques for multiphase

2.1.1 Lagrangian particle

The schematic illustration of the model is shown in Fig.1. As shown in Fig.2, this scheme uses a staggered grid system and has two kinds of Lagrange particles, i.e. SPH particles [8] denoted by gray dots and free surface particles denoted by black dots having physical properties, e.g. density and velocity. A solid model is represented by the SPH particles, which are characterized by density and their radius in order to compute ship motion and deformation.

Elastic deformation and fracture of ship motion can be computed by using the SPH particles. The free surface particles defined on Eulerian grid are located near free surface to capture accurately an interface between different phases, e.g. water surface. The free surface particles have density function ϕ_p to characterize physical properties at each phase. Density function ϕ_I is defined on node point of the staggered grid and it plays an important role of tracking the interface between different phases, such as air, water and solid.

Although particles in both sides of the interface are located in Particle Level Set Method [9], the free surface particles in this model are appropriately placed in only one side of free surface to reduce computational cost and time in redistribution process of the free surface particles.

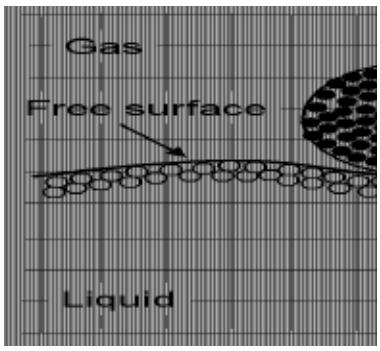

Fig.1 Grid arrangement and particle distribution (● : SPH particles, ○ : Free surface particles)

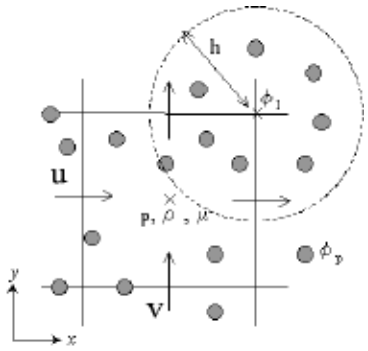

Fig.2 Definition of physical values on a grid and Lagrangian particles

2.1.2 Time evolution of Lagrangian Particles and Interpolation of physical value

Particle location on free surface is integrated by using evolution of the fourth order accurate Runge-Kutta method, following the evolution equation:

$$\frac{d\vec{x}_p}{dt} = \vec{u}(\vec{x}_p) \tag{1}$$

where $\vec{x}_p$ is the particle location, $\vec{u}(\vec{x}_p)$ is the particle velocity calculated by interpolating velocity on neighboring cell faces of grid. Meanwhile, SPH particles are placed in the area of solid phase and are advanced from the equation of rigid motion by using SPH method described in the following section.

Velocity components are defined on cell faces of grids and pressure in all phases is defined at the center as shown in Fig.2. Velocity of the free surface particle is interpolated from velocities on the neighboring cell faces of the grids by using bilinear in 2D or trilinear interpolation in 3D depending on the required accuracy and efficiency. For this simplifying reason, the number of particle can be corrected in one grid. In addition, Lagrange particles (SPH particles and free surface particles) are advected to maintain density function of the particle ϕ_p during calculation.

2.1.3 Redistribution of free surface particles

Using the model, in order to capture interface accurately during a calculation, redistribution of free surface particles is periodically needed to add and delete the particles using the technique developed by Enright et al. [9]. Figure 3 shows one example of the particle distribution for water entry problem of a circular obstacle in 2D. The particles are located near the free surface characterized by density functions. Using the redistribution process, both computational efficiency and stability are enhanced as well.

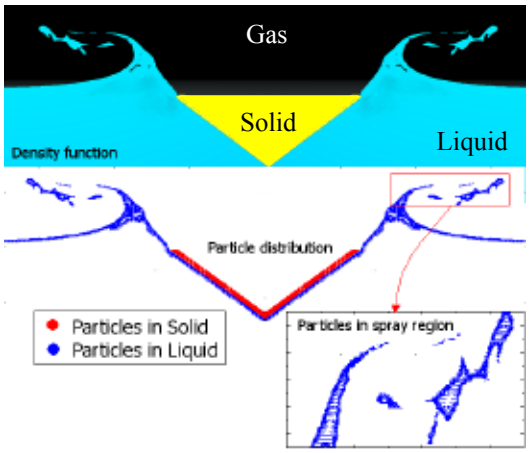

Fig.3 One example of particle distribution in water entry problem of a circular obstacle

2.1.4 Correction of density function on grids

In the model, density function ϕ_I defined on a grid node is corrected by using density function ϕ_p on free surface particles within referenced area with radius *h*. The density function ϕ_p reduces a numerical error generated in advection process using the following equation:

$$\phi_I' = \max\left(\phi_I \, , \sum_{j=1}^{N} \phi_p \frac{m_p}{\rho_p} W_p\left(\left|x_g - x_p\right|, h\right) \right) \tag{2}$$

where ϕ_I' is the density function on the node of the grids after the error correction, m_p / ρ_p is the particle volume, V_p is characterized by the particle radius r_p, W_p is the Kernel function defined as a cubic spline function, x_g and x_p are represented as spatial positions on a grid and a particle, respectively.

2.2 Governing equations and computational scheme

In the model, the governing equations for fluid phase consist of the mass conservation equation, incompressible Navier-Stokes equation and the equation of continuity, *I*-phase density function ϕ_I ($0 \le \phi_I \le 1$) and its advection equation. The equations are expressed as follow:

$$\frac{\partial \overline{u}_i}{\partial x_i} = 0 \tag{3}$$

$$\frac{\partial \overline{u}_i}{\partial t} + \overline{u}_j \frac{\partial \overline{u}_i}{\partial x_j} = -\frac{1}{\rho}\frac{\partial \overline{P}}{\partial x_i} - \frac{\partial \tau_{ij}}{\partial x_j} + \frac{\mu}{\rho}\frac{\partial^2 \overline{u}_i}{\partial x_j \partial x_j} + g_i + \overline{F}_{fsi} \tag{4}$$

$$\frac{\partial \phi_I}{\partial t} + \overline{u}_j \frac{\partial \phi_I}{\partial x_j} = 0 \tag{5}$$

where *I*-phases means gas-phase (I = 1), liquid-phase (I = 2) and solid-phase (I = 3), g_i is the gravity, F_{fsi} is the fluid structure interaction term, τ_{ij} is the SGS stress term. To reduce the model parameter, the SGS stress term is solved by using the LES model. In addition, the density function ϕ_I is used to identify physical properties of different phase and the density and the viscosity can be derived by using the density function ϕ_I as the following equations:

$$\rho = \sum_{I=1}^{3} \rho_I \phi_I \qquad \mu = \sum_{I=1}^{3} \mu_I \phi_I \tag{6}$$

The density function ϕ_3 (solid phase) is corrected by using Eq. (2) with SPH particles defined in solid phase.

The governing equations are solved using the splitting method as a well-known conventional multiphase technique. In the model, we use the C-CUP method developed by Yabe et al. [10] as the splitting method..

The governing equations for solid phase, which are discretized using the SPH method in the model, are the continuity equation and momentum equation as follows:

$$\frac{D\rho}{Dt} + \rho \frac{\partial u^i}{\partial x^i} = 0 \tag{7}$$

$$\rho \frac{Du^i}{Dt} = \frac{\partial \sigma^{ij}}{\partial x^j} + g^i - F^i_{fsi} \tag{8}$$

where ρ is the density, u^i is the velocity, x^j is the position vector of vector j components, σ^{ij} is the stress tensor of the solid phase, and F_{fsi} is the fluid structure interaction term. The stress tensor σ_s^{ij} in Eq.(8) is given by

$$\sigma_s^{ij} = -P\delta^{ij} + S^{ij} \tag{9}$$

where S^{ij} is the deviatoric stress tensor, $P = -\sigma_{kk}/3$ the pressure solved by the poisson equation.

The model considers a large deformation of an elastic body. The stress of a solid body changes at every calculation step by using the following equation:

$$\{dS^{ij}\} = [D^{ep}]\{d\varepsilon^{ij}\} \tag{10}$$

where D^{ep} is the elastic-plastic matrix, $d\varepsilon^{ij}$ the time increment of the strain, and dS^{ij} the time increment of the deviatoric stress.

To solve rotation of the solid phase during a deformation, the Jaumann derivative is used to ensure material frame indifference with respect to the rotation as follow:

$$\frac{dS^{ij}}{dt} = 2\mu\left(\dot{\varepsilon}^{ij} - \frac{1}{3}\delta_{ij}\dot{\varepsilon}^{ij}\right) + S^{ik}\Omega^{jk} + \Omega^{ik}S^{kj} \tag{11}$$

where $\dot{\varepsilon}$ is the strain rate tensor and Ω the spin tensor.

The fluid structure interaction F_{fsi} is solved by acceleration obtained from the pressure on the SPH particles interpolated using the pressure on grids solved by the Poisson equation (8). In the model, the fluid structure interaction F_{fsi} in Eqs.(4) and (8) can be given by the following equation:

$$F_{fsi}(\mathbf{r}_a) = -\frac{1}{\rho(\mathbf{r}_a)}\sum_b m_b \frac{P(\mathbf{r}_b)}{\rho(\mathbf{r}_b)} \nabla_a W(\mathbf{r}_a - \mathbf{r}_b, h) \tag{12}$$

To keep computational efficiency and stability, the time increment in the solid phase is approximately 1/10 to 1/50 of that in fluid phase.

The boundary condition for velocity on a solid body is imposed using the following equation:

$$u_b = \phi_3 \overline{u}_s + (1 - \phi_3) u_g \tag{13}$$

where u_b is the velocity on the Eulerian grid where the SPH particle on the surface of the tanker is located, ϕ_3 the density function of solid phase, $\overline{u}_s$ the velocity on the SPH particle in

each grid, u_g the velocity at the face of grid. This equation means that no-slip boundary condition is imposed on the surface of the solid body.

2.3 Solid motion in 3D

In the model, a solid model consists of SPH particles to capture motion and deformation of a ship. Therefore, the 3D motion of a ship hull is represented by describing translation and rotation of the center of gravity of a solid using the following equations:

$$\frac{\partial^2 x_{s,k}}{\partial t^2} = \frac{F_{s,k}}{m_i} - F_{fsi} \tag{14}$$

$$I\frac{\partial \omega_i}{\partial t} = T_i \tag{15}$$

$$\frac{\partial \theta_i}{\partial t} = \omega_i \tag{16}$$

where θ_i is the rotational angle, ω_i is the angular velocity, T_i is the torque, I is the inertia moment, and F_{fsi} is the fluid structure interaction. In addition, the center of gravity of the ship hull can be obtained by calculating the inertia moment of SPH particles, and this is calculated by using Baraff theory [11]. Based on this theory, in the model, the equations for the 3D motion are given by

$$\mathbf{r}_g = \frac{1}{N}\sum_{i=1}^{n}\mathbf{r}_i \qquad I = \sum_{i=1}^{N} m\left|\mathbf{r}_i - \mathbf{r}_g\right|^2 \tag{17}$$

where N is the coordinate of the center of gravity of a solid body. $\mathbf{r}_g$ is the position of the gravity center, I is the inertia moment, $\mathbf{r}_i$ is the position of the ith SPH particle and m is the mass of the particle. We can represent time integration of the location of the rigid body by the following equations:

$$\hat{\mathbf{r}}_i' = \hat{\mathbf{r}}_i^{k+1} - \mathbf{r}_i^k \tag{18}$$

$$\mathbf{r}_g^{k+1} = \frac{1}{N}\sum_{i=1}^{N}\hat{\mathbf{r}}_i^{k+1} \tag{19}$$

$$\mathbf{r}_g' = \frac{1}{N}\sum_{i=1}^{N}\hat{\mathbf{r}}_i' \tag{20}$$

$$\theta' = \omega dt = \frac{1}{I}\sum_{i=1}^{N} m\hat{\mathbf{r}}_i' \times (\mathbf{r}_i^k - \mathbf{r}_g^{k+1}) \tag{21}$$

$$\mathbf{r}_i' = \mathbf{r}_g' + \mathbf{R}^{-1}(\mathbf{r}_i^k - \mathbf{r}_g^{k+1}) \tag{22}$$

$$\mathbf{u}_i^{k+1} = \frac{\mathbf{r}_i'}{\Delta t} \tag{23}$$

$$\mathbf{r}_i^{k+1} = \mathbf{r}_i^k + \mathbf{r}_i' \tag{24}$$

where the R is a 3×3 rotation matrix. We also use the unit quaternion instead of rotation matrices. The inertia moment is set at initial condition. Therefore, the coordinates of velocity of each SPH particle in every time step can be tracked by using the rotation matrix and the amount of the angle rotation of the center of gravity to avoid the Gimbal lock phenomenon, and the quaternion is used instead of the rotation matrix.

3 NUMERICAL RESULTS

3.1 Water entry problem of elastic cylinder

We applied to a water entry problem of an elastic cylinder made of polyvinylchloride plastic as a benchmark test to validate the developed numerical model. As shown in Figure 4, the diameter is 15cm and the length is 13.5mm and the thickness is 15mm. The Young modulus is 3400MPa and the poison ratio is 0.38 and the density is 1,700kg/m^3. The inner strain of the elastic cylinder at three different points (Point.1 to 3) was measured by PVDF film. The initial entry speed is 2.8m/sec. The position of the elastic cylinder was captured by high speed camera (1000fps).

Figure 5 shows snapshots of the water entry process captured by the high speed camera. Figure 6 shows time history of the strain on the inner face of the elastic cylinder. All of the time histories of strain are damping oscillation which corresponds to the natural frequency of the submerged elastic cylinder. The frequency spectrum of the strain during the entry process is shown in Fig.7. In this case, the dominant frequency is about 175Hz.

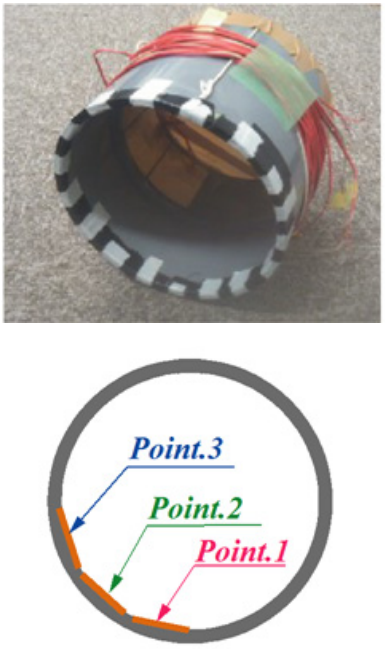

Figure 4 : Elastic cylinder model and strain measuring points at the inner surface.

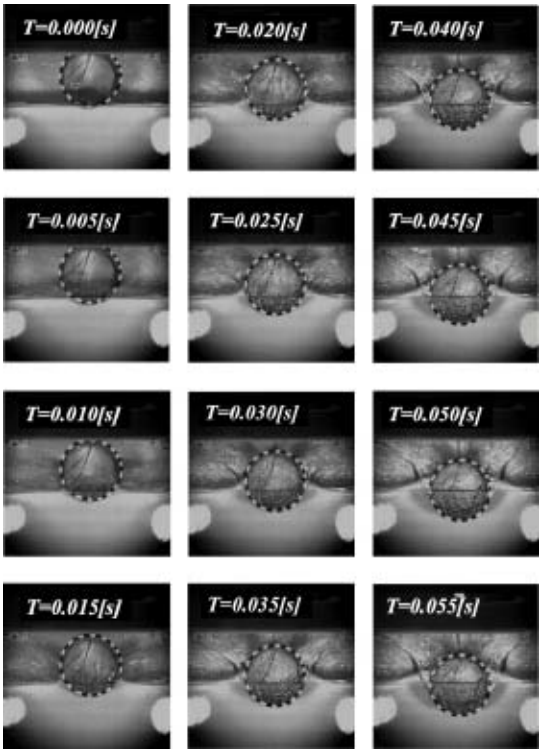

Figure 5 : Snapshots of the elastic cylinder during the entry process in the experiment.

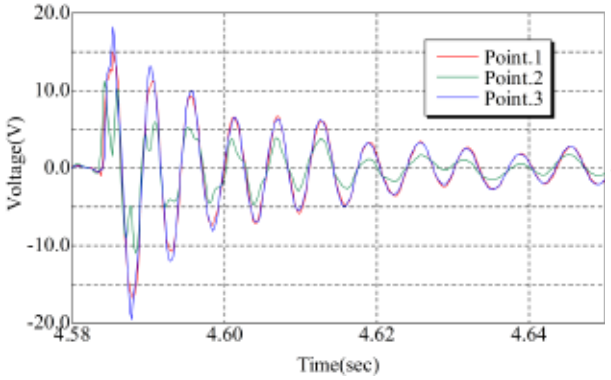

Figure 6 : Time history of strain at the inner face of the elastic cylinder during the entry process in the experiment.

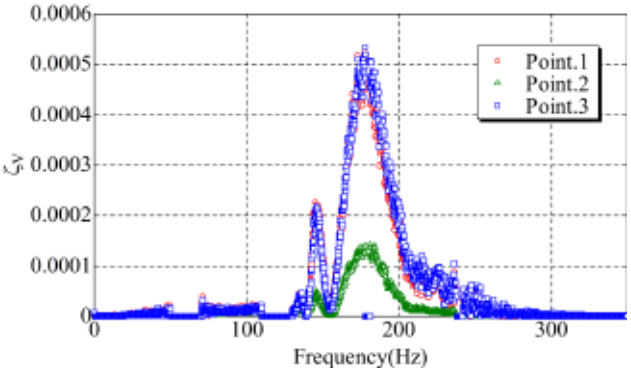

Figure 7 : Dominant frequency of the strain in the experiment.

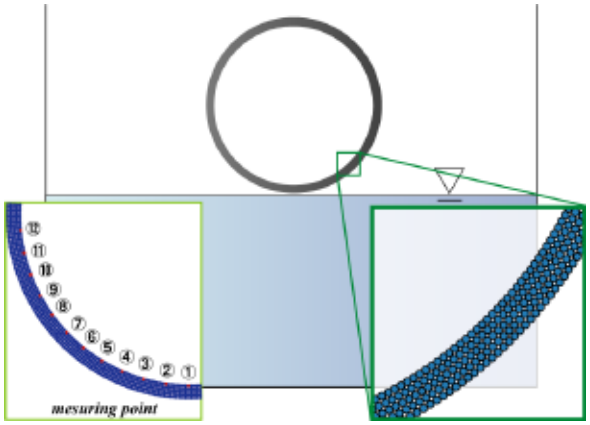

Figure 8 : Initial conditions of water entry problem and particle distribution in the elastic cylinder.

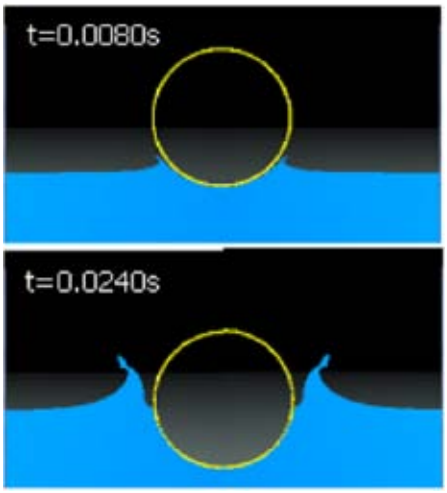

Figure 9: Water entry process of the elasticc cylinder

To validate the developed numerical model, the entry process in 2D was computed with the initial conditions as show in Fig.8. The elastic cylinder consists of the SPH particles that the total number is 1,885 and its radius is 0.31mm. The free surface particles are located near the free surface and its radius is 0.75mm. The total number is 7,224. The grid size is 3mm and the total grid number is 120,000 in 2D. The monitoring points (Pt.1 to 12) are located at the inner face of the cylinder to compare the strain of the elastic cylinder with the experimental result.

Figure 9 shows the entry process of the elastic cylinder into the still water. It can be seen that the strongly splashing was generated from the thin layer between the cylinder and the water. Figure 10 shows the comparison of the vertical position of the cylinder between the experiment and the numerical result. The numerical result is overall agreement with the experimental one. Figure 11 shows the time history of the strain at the inner face of the

cylinder during the water entry process. The dominant frequency is shown in Fig.12. The frequency is about 180Hz which coincides with the experimental result as shown in Fig.7. We investigated the internal strain of the elastic cylinder during the entry process as shown in Fig.13. The internal strain during the entry is rapidly exchanged in time and space.

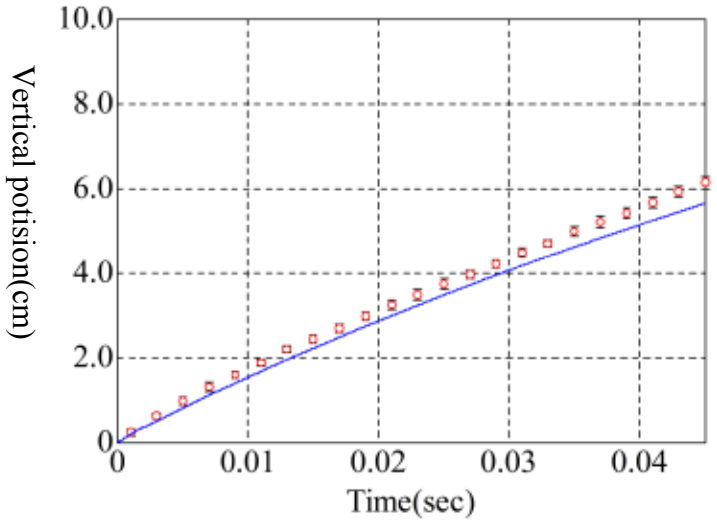

Figure 10: Comparison of vertical position of the elasticc cylinder during the entry process. (dots : experiment, solid line : numerical result)

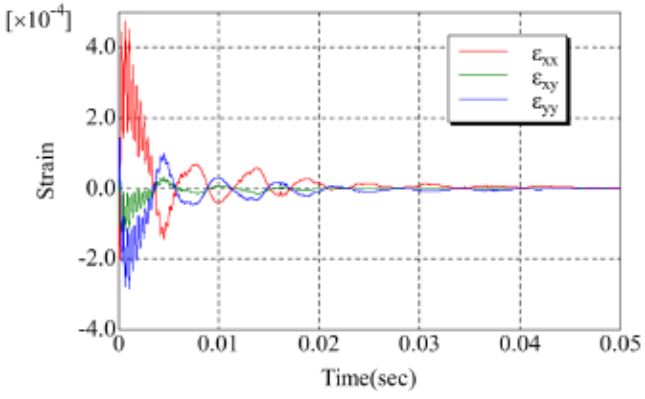

Figure 11: Time history of strain at the inner face of the elastic cylinder during the water entry process in numerical result.

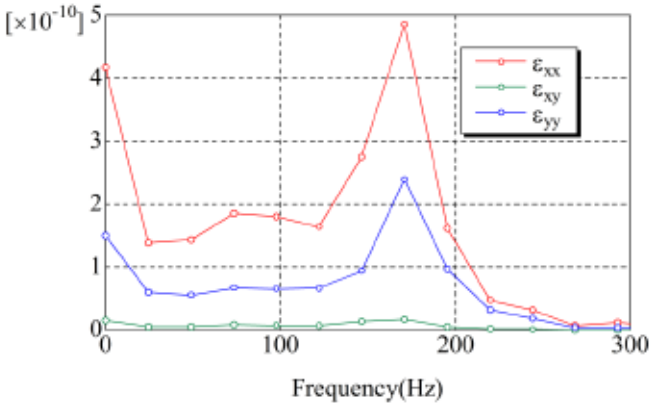

Figure 12: Dominat frequency of the strain in numerial result.

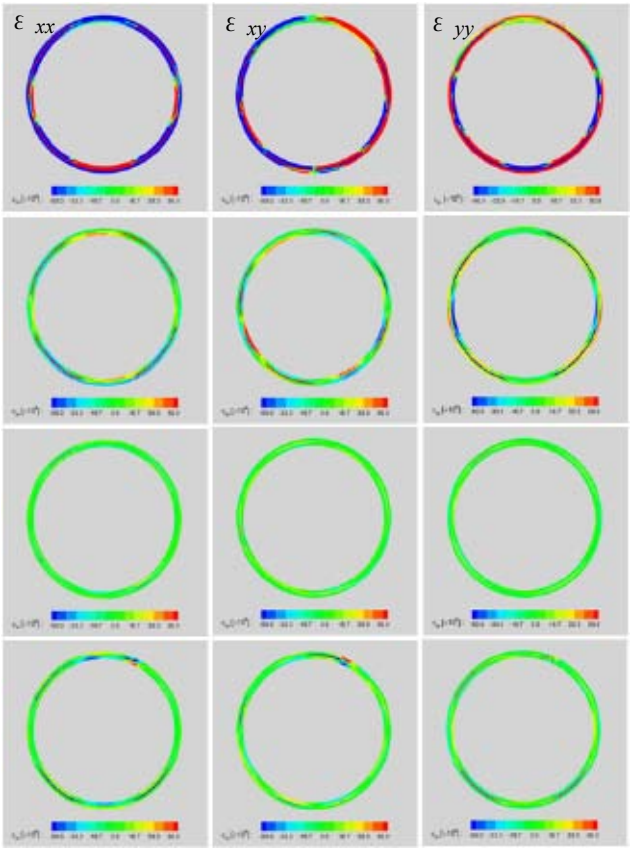

Figure 13: Internal strain field of the elastic cylinder during the entry process

3.3 Elastic ship body in wave

We applied to numerical simulation of an elastic ship motion in regular wave. Figure 14 shows the bird's-eye view of the ship hull as a tanker type. As shown in the previous section, in the model, the tanker is represented by a large number of the SPH particles traced by particle based method, SPH. The incident wave height is H_w / L_{pp}=0.06 and the wave length is λ / L_{pp}=1.0. The *Fr* number is 0.226 at the initial condition. The grid size is 0.0025 L_{pp} and the radius of free surface particle is 0.0025 L_{pp}. The total number of the free surface particle located near free surface is 1,300,000. The radius of the SPH particle is 0.0025 L_{pp} and the total number is 26,000 for the tanker.

Figure 14 Distribution of SPH particle on a tanker

Figure 15 shows snapshots of the freely elastic tanker motion in head sea of regular waves. These results show that heave and pitch motions of the tanker in head sea of regular wave can be seen, and also there are the strongly nonlinear phenomena such as splashing, breaking, slamming and green water with the tanker motion. Figure 16 shows the strain distribution of the elastic tanker in the regular wave. It can be seen that the hogging and sagging motions were occurred under the impact load due to the strongly nonlinear phenomena such as slamming and green water. Figure 17 shows the time history of the strain at the three different points on the deck and bottom. The high frequency strain was generated by the hogging and sagging motions on both faces.

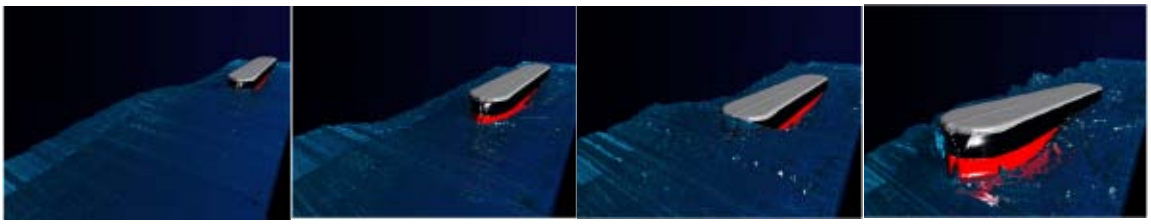

Figure 15 Snapshots of freely elastic tanker motion in head sea of regular wave.

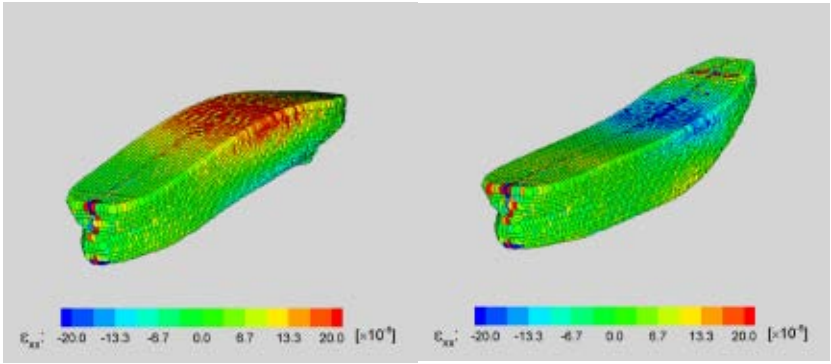

Figure 16 Deformation and Strain distribution of the elastic tanker under the hogging and sagging motions.

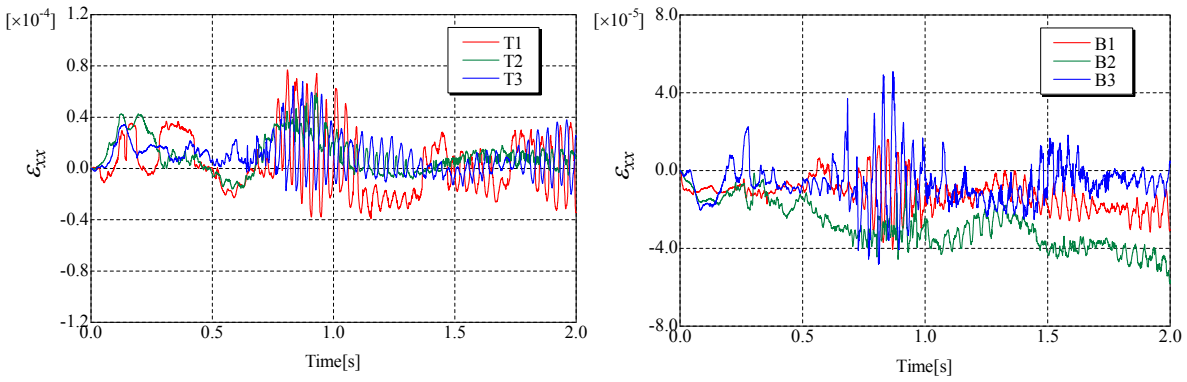

(a) Deck (b)Bottom

Figure 17 Time history of strain on the deck and bottom under the hogging and sagging motions.

4 CONCLUSIONS

To investigate hydroelastic phenomena caused by water impact, we have developed a coupled Eulerian scheme with Lagrangian particles to combine advantages and to compensate disadvantages in both grid based method and particle based method. The developed numerical model was applied to hydroelastic problems due to impact pressure such as water entry of the elastic cylinder and the elastic tanker motion in wave. The numerical results are in good agreement with the experimental result. This numerical model can be useful and effectiveness to evaluate hydroelasticity and motion of a body in a structure design process. More detailed validation will be necessary as future work.

ACKNOWLEDGEMENT

The authors would like to be grateful to Mr. Kurokawa in HITACHI, Ltd who partly computed the numerical results.

REFERENCES

[1]Haugen, E. M., "Hydroelastic analysis of slamming on stiffened plates with application to catamaran wetdeck", *Ph.D Thesis, Dept. Marine Hydrodynamics*, NTNU, 170p (1999).

[2]Meyerhoff, W. K., "Added mass of thin rectangular plates calculated from potential", *Journal of Ship Research*, pp.110-111 (1970).

[3]Faltinsen, O. M., "Water entry of a wedge by hydroelastic orthotropic plate theory", *Journal of Ship Research*, **43**, pp.180-193 (1999).

[4]Faltinsen, O. M., "Hydroelastic slamming", *Journal of Marine Science and Technology*, pp.49-65(2000).

[5] Mutsuda, H. and Shinkura, Y. and Doi, Y., "An Eulerian scheme with Lagrangian particles for solving impact pressure caused by wave breaking", *Proc. of the 18th International Society of Offshore and Polar Engineers Conference*, Vol.3, pp.162-169 (2008).

[6] Mutsuda, H, Shimizu, Y and Doi, Y., "Numerical Study on Interaction Between Violent Wave and Structure Using SPH", *Particle-Based Methods, Fundamentals and Applications, PARTICLES* 2009, Barcelona, pp. 266-269 (2009).

[7] Mutsuda, H, Kurokawa, T, Baso, S and Doi, Y., "Numerical Simulation of Interaction Between Wave and Floating Body Using Eulerian Scheme with Lagrangian Particles", *Proc IV European Conference on Computational Mechanics (ECCM2010)*, Paris, CD-Rom (2010).

[8]Gingold, R.A., and Monaghan, J.J., "Smoothed particle hydrodynamics, theory and application to non-spherical stars, *Mon. Not. Roy. Astr. Soc.*, Vol. 181, pp.375-389 (1977).

[9] Enright, D., R. Fedkiw, J. Ferziger, I. Mitchell, "A hybrid particle level set method for improved interface capturing", *J. Comput. Phys*., 183(1), pp.83-116 (2002).

[10]Yabe, T. and Wang, P.Y. "Unified numerical procedure for compressible and incompressible fluid", *Journal of the Physical Society of Japan*, Vol.60, No.7, pp.2105-2108 (1991).

[11]Barraf, D., "An introduction to physically based modeling,: Rigid body simulationI ~Unconstrained rigid body dynamics~, *SIGGRAPH'97 course note*, D3 (1997).